The paper was published in the proceedings of the 11th International Conference on Physical Modelling in Geotechnics (ICPMG2026) and was edited by Ioannis Anastasopoulos. The conference was held from June 8th to June 12th 2026 in Zurich, Switzerland.

Proceedings of the 11th ICPMG 2026
11th International Conference on Physical Modelling in Geotechnics
8-12 June 2026, Zurich, Switzerland

Impact of groundwater table fluctuations on uplift and bearing capacities of short straight-shaft and spiral piles under two-way cyclic loading

F. Shah
Faculty of Engineering, Hokkaido University, Sapporo, Japan, faheemshahm07@gmail.com

K. Isobe
Faculty of Engineering, Hokkaido University, Sapporo, Japan, kisobe@eng.hokudai.ac.jp

ABSTRACT: The growing demand for renewable energy has accelerated solar power installations, often on soft or sloped ground where short spiral (helical) piles are preferred for their strong uplift resistance and ability to reinforce slopes through rotational penetration. These piles are also widely used in subway platform door foundations. However, fluctuations in the groundwater table (GWT) can significantly influence their axial performance. This study experimentally examines the effects of GWT variations on the uplift and vertical bearing capacities of short straight-shaft and spiral piles subjected to two-way cyclic loading. Initial tests in fully saturated silica sand established baseline behavior. Lowering the GWT increased both uplift and bearing capacities due to soil desaturation, enhanced matric suction, and greater effective stress, improving soil-pile interaction. The spiral pile, which mobilizes additional shaft friction along its helical blades, exhibited a more pronounced capacity increase than the straight-shaft pile. Under unsaturated cyclic loading, both piles experienced performance degradation caused by suction-maintained gaps forming around the pile, reducing tip and shaft resistances. Upon re-saturation, suction dissipated and sand flowed into these gaps, restoring soil-pile contact and resulting in bearing capacity recovery. Although the recovered capacity remained lower than under unsaturated conditions, it exceeded the initial saturated state due to localized densification and enhanced interparticle interlocking from prior cyclic loading. These findings highlight the critical role of suction and re-saturation processes in governing pile behavior under cyclic loading and emphasize the need to incorporate groundwater fluctuation effects in the design of short piles for solar panels.

1 INTRODUCTION

In recent years, the growing demand for renewable energy has significantly accelerated the construction of solar power generation infrastructure. These infrastructures are often installed on low-valued land with poor ground conditions. Foundation options for solar systems can be categorized based on their installation methods into several groups: direct drilled concrete piers, excavated and backfilled precast concrete piers, excavated and backfilled cast-in-place concrete piers, cast-in-place footings, driven piles, and helical piles (Lutenegger, 2016). Each of these methods offers distinct advantages depending on the specific ground conditions and project requirements. For soft ground conditions, small-diameter and short-length steel pipe piles, spiral piles, and diagonal piles have demonstrated significant potential in enhancing stability and performance (Hirata et al., 2005; Araki, 2013; Sato et al., 2015; Nakagawa et al., 2018; Tamboura et al., 2022). Among these alternatives, the screw pile is more popular due to its rapid installation, immediate load-bearing capacity, minimal waste production, eco-friendliness, suitability for narrow spaces and reusability (Zhou et al., 2023; Ho et al., 2022; Cerfontaine et al., 2020; Ullah et al., 2019).

The screw pile installation is characterized by advancement ratio (AR) (Bradshaw et al., 2018; Sharif et al., 2021). Which is the ratio of pile vertical displacement (Δz_h) to the pitch of the screw pile (p_h) per rotation. Mathematically advancement ratio (AR) can be calculated as:

$$\mathrm{AR} = \Delta z_h \, / \, p_h \qquad (1)$$

The advancement ratio (AR) of 1±0.15 is recommended by code of practice for foundations London, UK (BSI, 2015). Perko (2009) recommended that the advancement ratio (AR) of a screw pile should exceed 0.8. These indicate that the pile should advance by one helix pitch per revolution of the helix. This specific installation practice, known as 'pitch-matched' is intended to minimize soil disturbance during installation, which is often deemed detrimental to the surrounding soil and overall pile performance (Cerfontaine et al., 2023).

The loading and unloading cycles experienced by helical anchors during their service life can alter the soil characteristics around the anchor. As a result, the performance of the helical anchor may vary with the cycles of wind loading. Shah et al. (2024) investigated the cyclic response of continuous screw piles embedded in saturated and unsaturated sandy ground under two-way cyclic loading. Their study revealed that, in unsaturated sand, a cyclic loading-induced gap developed between the pile tip and the surrounding soil during load reversal. This occurred because matric suction held the soil grains together, preventing sand from flowing downward to refill the space when the load changed from compression (push-in) to tension (pull-out). As a result, a small void remained under the pile tip and around the shaft, reducing the effective contact area and thereby decreasing tip resistance and shaft friction during the subsequent compression phase. Consequently, a gradual reduction in bearing capacity was observed with an increasing number of load cycles.

In contrast, under saturated conditions, no such gap formation or cyclic degradation of tip resistance was reported. In saturated sand, the presence of free water allowed soil particles to flow into any void that might form during uplift, thereby maintaining or even improving contact between the pile and the surrounding soil. This led to localized densification beneath the pile tip, contributing to more stable or enhancing tip resiatnace behaviour with continued cycling.

Building upon the findings of Shah et al. (2024), the present study aims to further investigate the effect of resaturation on the cyclic response of piles. Specifically, this research explores whether the gap formed during cyclic loading in unsaturated soil can be closed once the soil is resaturated, through the loss of suction and subsequent soil flow into the previously formed void.

To achieve this, controlled laboratory experiments were conducted on both straight-shaft (normal) and spiral piles installed in sandy soil. The same model ground was sequentially subjected to three stages: (i) cyclic loading under initially saturated conditions to establish baseline behavior, (ii) cyclic loading under unsaturated conditions to induce a cyclic gap, and (iii) re-saturation of the model ground followed by cyclic loading to evaluate the recovery of soil-pile contact and load-bearing behavior.

2 OUTLINE OF MODEL TEST

2.1 Model piles

In this study, two types of model piles were examined: a conventional straight pile (NP12) and a spiral pile (SP30). The conventional pile (NP12) is a smooth cylindrical pile with a diameter D_P = 12 mm. The spiral pile (SP30) has the same shaft diameter (D_P = 12 mm) but is equipped with a helical (continuous spiral) blade having an outer diameter D_W = 25 mm, as illustrated in Figure 1.

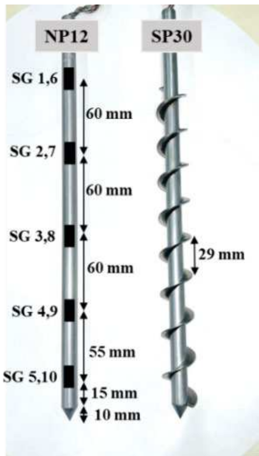

Figure 1. Model piles.

The spiral blade was fabricated from a thin metal strip and firmly bonded to the circumferential surface of the straight pile using industrial adhesive. The blade follows a right-hand winding pattern with a pitch of 29 mm, extending along the entire shaft except at the pile tip. For analytical purposes, the effective surface area and end-bearing area of the spiral pile were conservatively estimated assuming a uniform diameter of 25 mm. This assumption yields a lower-bound (conservative) estimation of the pile's end-bearing pressure. It is acknowledged, however, that the actual effective diameter of the spiral pile likely lies between 12 mm and 25 mm, and further research is required to determine its true bearing area more accurately. Nevertheless, adopting a conservative approach is deemed appropriate for the current stage of investigation to ensure safe and consistent comparison with the conventional pile.

To monitor the axial force distribution**,** two strain gauges (SGs) were installed at each of five cross-sections along the length of both pile types (see Figure 1). The strain gauges were attached to the inner surface of the hollow aluminum piles to protect them from damage during installation. The locations of the gauges on the spiral pile (SP30) corresponded precisely to those on the conventional pile (NP12), ensuring comparable measurement conditions. The key physical and geometric properties of both piles are summarized in Table 1.

Table 1. Model piles data.

Properties	Units	NP12	SP30
Mass	kg	0.056	0.096
Total length	mm	313	313
Effective length	mm	260	260
Pile diameter D_P	mm	12	12
Wing diameter D_W	mm	-	25
Surface area	mm^2	9797	20410
Effective base area	mm^2	113	490.6
Wing pitch p_w	mm	-	29
Young's modulus	GPa	69.1	70.8

2.2 Model ground preparation

The experimental setup employed a cylindrical soil chamber (Figures 2 and 3) with an internal diameter of 300 mm and a depth of 630 mm. The model ground was prepared using Silica Sand No. 7, which was placed in 12 layers, each 30 mm thick, to achieve a total sand height of 360 mm. A relative density of 45% was obtained by the air pluviation method, where sand was poured from a height of 630 mm. The physical properties of the silica sand are summarized in Table 2.

To establish saturated conditions, water was slowly introduced from the bottom of the chamber, allowing upward infiltration through the sand layer. The water level was continuously monitored during infiltration, and once it reached the sand surface, the inflow was stopped. The water level was then maintained for a sufficient duration to allow complete saturation and equilibrium throughout the model ground.

Table 2. Silica sand No. 7 properties.

Physical property	Units	Silica sand
Particle density (ρ_s)		2.67
Maximum dry density (ρ_{dmax})	Mg/m^3	1.60
Minimum dry density (ρ_{dmin})		1.25

The unsaturated condition was created by first saturating the sand, followed by drainage using top-applied air pressure to expel pore water from the upper layers downward. This method effectively transitioned the sand bed from a saturated to an unsaturated state by bring water table to just above the porous stone. To monitor the pore pressure distribution, five pore water presssure gauges (WP) were embedded at different depths within the soil tank (Figure 3). The recorded pressure heads during the test are presented in Table 3. The experiments were conducted as 1-g small-scale model tests; therefore, the overburden stress level in the soil is relatively low, and matric suction may constitute a larger portion of the shear strength, potentially amplifying its influence. However, the practical target of this study is small-diameter, short pile foundations with an assumed embedment depth of ≤ 1.5 m. Because extremely high stress levels are not expected under such conditions, the scale-related influence of suction is likely to be limited.

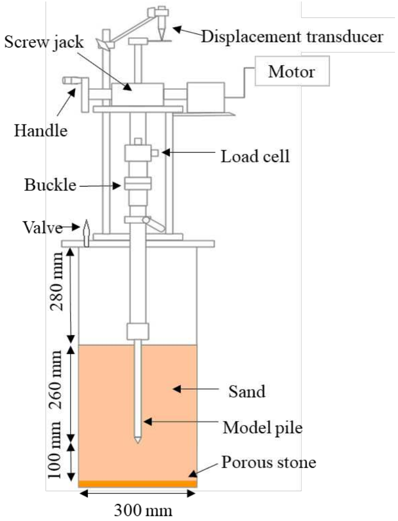

Figure 2. Cylindrical soil chamber with loading device.

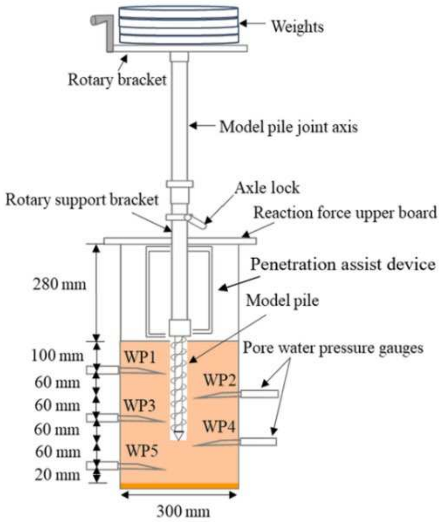

Figure 3. Cylindrical soil chamber with penetration device.

Table 3. Pore water pressure heads for NP12 and SP30.

Pressure head	WP1 (kPa)	WP2 (kPa)	WP3 (kPa)	WP4 (kPa)	WP5 (kPa)
NP12	-3.22	-2.31	-1.39	-1.10	-0.74
SP30	-2.05	-1.82	-0.69	-0.63	-0.15

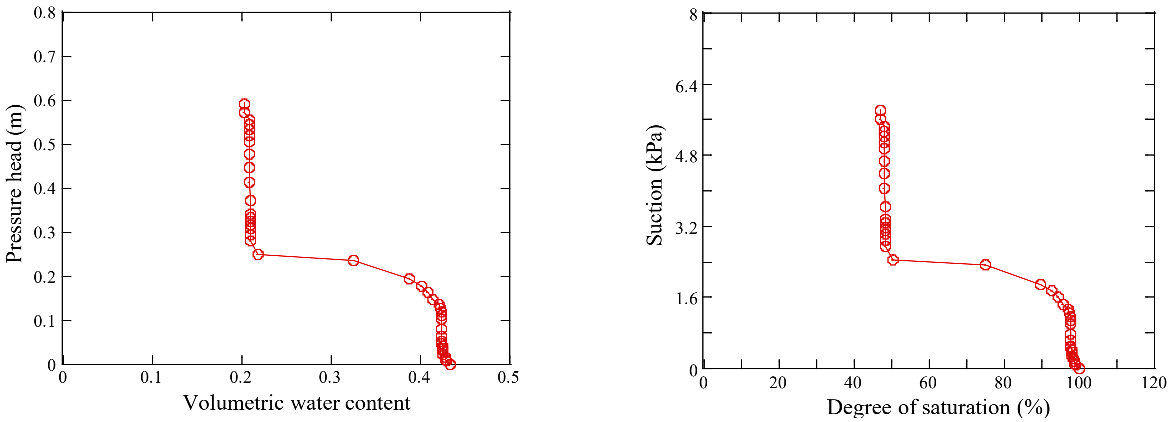

a) Volumetric water content vs pressure head (m) *b) Degree of saturation (%) vs suction (kPa)*

Figure 4. Soil water characteristics curve (SWCC)

Volumetric water content was estimated from the Soil Water Characteristic Curve (SWCC) obtained using the suction head method (Fig. 4a). The corresponding degree of saturation at each depth was then derived from the suction-water content relationship (Fig. 4b), allowing the soil moisture state to be quantified for both saturated and unsaturated conditions.

2.3 Pile installation procedure

For the normal pile (NP12), the pile was first released from a small height above the ground surface to allow free fall penetration under its own weight. However, this method alone did not achieve the target embedment depth of 260 mm. Therefore, a press-in method was adopted, wherein incremental vertical loads were applied to the top of the rotary bracket to advance the pile gradually. In each step, an additional load of 500 g was placed on the bracket, and the corresponding penetration depth was recorded. Once the pile reached approximately 80% of the target depth, a loading device (shown in Figure 2) was connected to the pile to apply controlled displacement, ensuring that the final penetration did not exceed 260 mm.

For the spiral pile (SP30), installation was carried out manually using a rotary bracket, as shown in Figure 3. Controlled installation was achieved with the aid of a jig (Figure 3), which ensured the advance ratio (AR) remained close to 1. A constant vertical load was simultaneously applied to the bracket to maintain a uniform penetration per rotation, corresponding to the pitch of the spiral blade (29 mm). This procedure enabled consistent downward advancement while minimizing disturbance to the surrounding sand.

2.4 Loading procedure

After installation, the loading device (Figure 2) was securely attached to the pile head. During the testing sequence, it was assumed that the pile initially experienced allowable bearing capacity conditions, followed by progression to ultimate bearing capacity conditions. The ultimate bearing capacity was defined as the point at which the vertical displacement reached 10% of the pile diameter (D_P) at the loading point.

To simulate the allowable bearing capacity condition, the piles were first subjected to two-way cyclic loading with displacement amplitudes corresponding to 2% of the pile diameter in both the push-in and pull-out directions. This cyclic loading was repeated for six cycles, maintaining a constant loading rate of 0.5 mm/min.

Following this stage, the piles were subjected to additional cyclic loading to reach the ultimate bearing capacity condition, characterized by a displacement amplitude of 10% of the pile diameter in both loading directions. This phase also consisted of six additional cycles, but at an increased loading rate of 2.5 mm/min, since the influence of loading rate was considered negligible within the test range.

3 RESULTS AND DISCUSSIONS

Figure 5 presents the relationship between load and normalized displacement (displacement divided by pile diameter) for both the normal pile (NP12) and the spiral pile (SP30). In every test, the spiral pile demonstrated a markedly higher vertical bearing capacity than the normal pile approximately five times greater in saturated conditions and nearly six times greater in unsaturated conditions. This superior performance is primarily attributed to the helical geometry of the spiral pile, which increases the available contact surface along the pile shaft. The spiral blade enhances soil-pile interaction by mobilizing higher circumferential resistance, thereby facilitating more efficient load transfer. Although the improvement in pull-out capacity is less pronounced than in vertical bearing, the spiral pile still outperforms the normal pile about three times higher in saturated and six times higher in unsaturated conditions (see Figure 5) due to its greater interface friction and enlarged contact area (refer to afermentioned Figure 7).

Under unsaturated conditions, the normal pile exhibited noticeable cyclic degradation in vertical bearing capacity (Figure 5b), primarily caused by a reduction in tip resistance during repeated loading (Figure 6b). A similar trend was observed for pull-out performance. The spiral pile in unsaturated conditions also showed degradation during the ultimate loading cycles (Figure 5e). This degradation is explained by the formation of a cyclic-loading-induced gap between the pile and surrounding soil, particularly beneath the pile tip. In unsaturated sand, suction-induced adhesive forces inhibit particle migration into the gap formed during load reversal, thereby temporarily reducing the effective contact area between the pile and surrounding soil. As a result, both tip and shaft resistances decrease until additional displacement is applied to re-establish full soil-pile contact. These observations are consistent with the behavior reported by Shah et al. (2024).

After completing the unsaturated cyclic tests, the soil was re-saturated, and twelve additional two-way loading cycles were applied. The corresponding load-displacement responses are shown in Figures 5c and 5f. Upon re-saturation, both pile types exhibited a distinct recovery in load-bearing capacity, reversing much of the degradation that had occurred under unsaturated conditions. This recovery is attributed to the dissipation of matric suction, which allowed sand particles to flow into the previously formed gaps, thereby restoring continuous soil-pile contact along both the tip and shaft. As the contact area expanded, tip and shaft resistances increased, resulting in a noticeable improvement in overall bearing performance. However, because suction loss reduced the apparent cohesion of the sand, the total bearing capacity remained lower than that under unsaturated conditions, even though no significant additional cyclic degradation occurred after re-saturation. Interestingly, both piles demonstrated slightly higher capacities compared with their initial saturated state, likely due to localized densification beneath the pile tip during the earlier unsaturated phase. Upon re-saturation, the rearrangement of sand into the cyclic-loading-induced gaps further enhanced interparticle contact, leading to a modest but measurable improvement in overall bearing capacity.

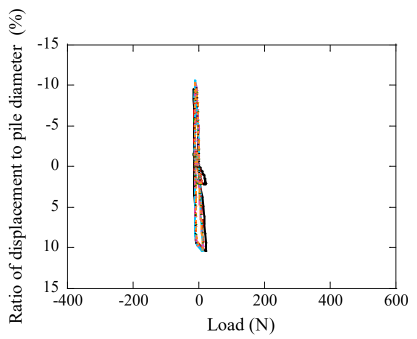

a) NP12 initial saturated condition

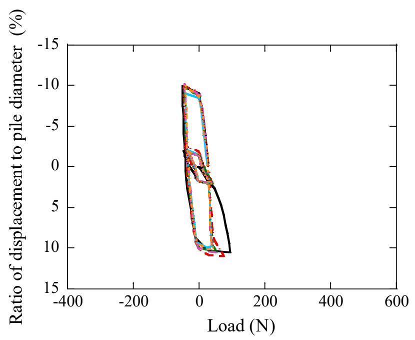

b) NP12 unsaturated condition

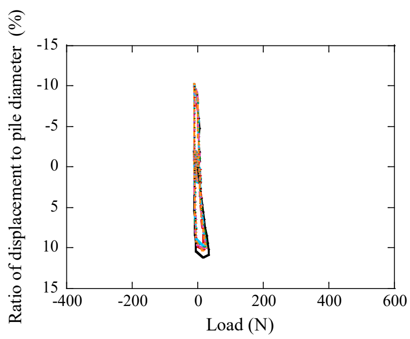

c) NP12 re-saturated condition

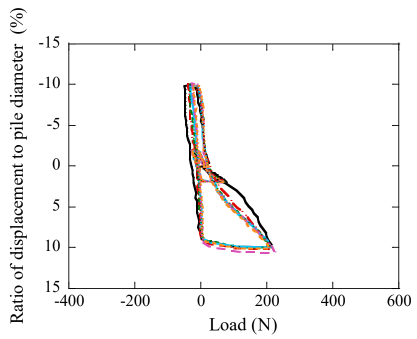

d) SP30 initial saturated condition

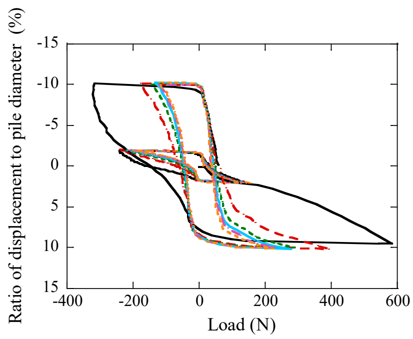

e) SP30 unsaturated condition

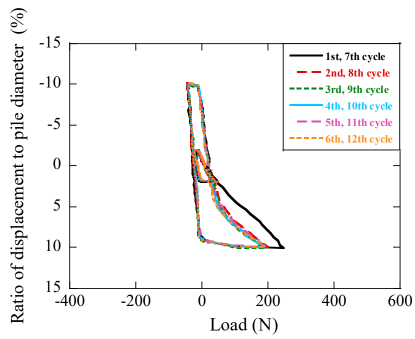

f) SP30 re-saturated condition

Figure 5. Load vs displacement ratio of NP12 and SP30 in saturated, unsaturated, and re-saturated sandy ground.

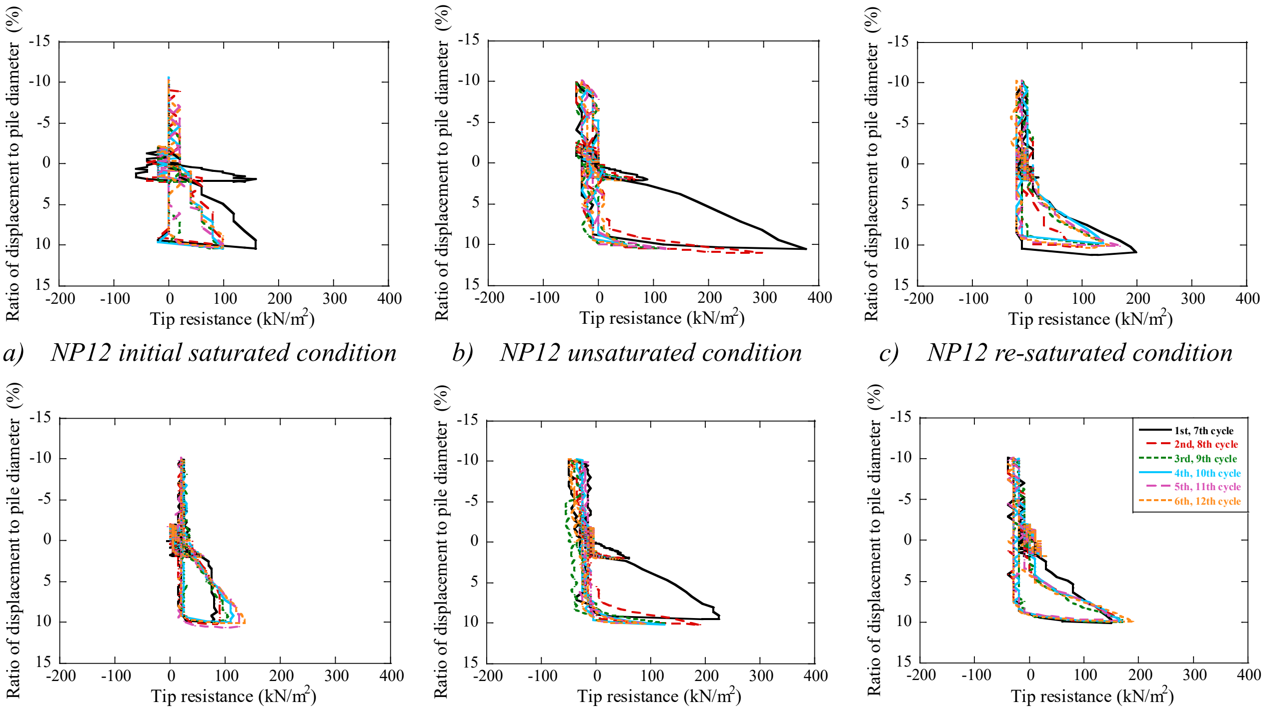

a) NP12 initial saturated condition *b) NP12 unsaturated condition* *c) NP12 re-saturated condition*

d) SP30 initial saturated condition *e) SP30 unsaturated condition* *f) SP30 re-saturated condition*

Figure 6. Tip resistance vs displacement ratio of NP12 and SP30 in saturated, unsaturated, and re-saturated sandy ground.

Figure 6 presents the relationship between tip resistance and normalized displacement (displacement divided by pile diameter) for both pile types. The effective bearing area of the spiral pile was conservatively estimated by assuming a 25 mm diameter, although the actual effective diameter likely lies between 12 mm and 25 mm. Further investigation is needed to accurately evaluate the effective bearing area of spiral piles. Nevertheless, this conservative assumption provides a safe lower-bound estimation of end bearing pressure for the current analysis.

For the normal pile (NP12), the tip resistance in unsaturated conditions was found to be higher than in saturated conditions during the loading cycles. However, under cyclic loading, the tip resistance exhibited progressive degradation in both cases. In saturated sand, the degradation stabilized after the first cycle of the ultimate loading phase, and the resistance remained relatively constant thereafter. In contrast, under unsaturated conditions, the degradation was more pronounced, leading to a near-complete loss of tip resistance up to approximately 5 to 7% normalized displacement (refer to Figure 6b).

The spiral pile (SP30) displayed a similar degradation trend under unsaturated conditions, particularly after the first cycle of each loading sequence (see Figure 6e). The sharp reduction in tip resistance indicates the formation of a cyclic-loading-induced gap between the pile tip and the surrounding soil. The cyclic-loading-induced gap forms due to the asymmetric soil response during push-in and pull-out. When the pile is pushed downward, the soil beneath the tip compresses and densifies. During pull-out, the soil does not rebound, and because the unsaturated sand lacks sufficient water for particle flow, no soil movement occurs to fill the void, resulting in a persistent gap between the pile tip and the soil. Once this gap formed, matric suction in the unsaturated sand maintained the separation, preventing sand particles from flowing back into the gap. Consequently, the pile experienced limited tip resistance until larger displacements were applied, confirming that the gap formation and suction retention play a critical role in governing the tip resistance behaviour under unsaturated conditions.

Upon re-saturation, the matric suction dissipated, allowing sand particles to flow and fill the cyclic-induced gap. When subsequent loading cycles were applied, the contact area between the soil and pile tip increased relative to the unsaturated condition, leading to a marked recovery in tip resistance. Moreover, since the sand had undergone localized densification during the prior unsaturated stage, the closure of the gap further enhanced particle interlocking beneath the pile tip. As a result, both the normal and spiral piles exhibited higher tip resistance after re-saturation than in their initial saturated states, although the tip resistance remained lower than that observed under unsaturated conditions (see Figures

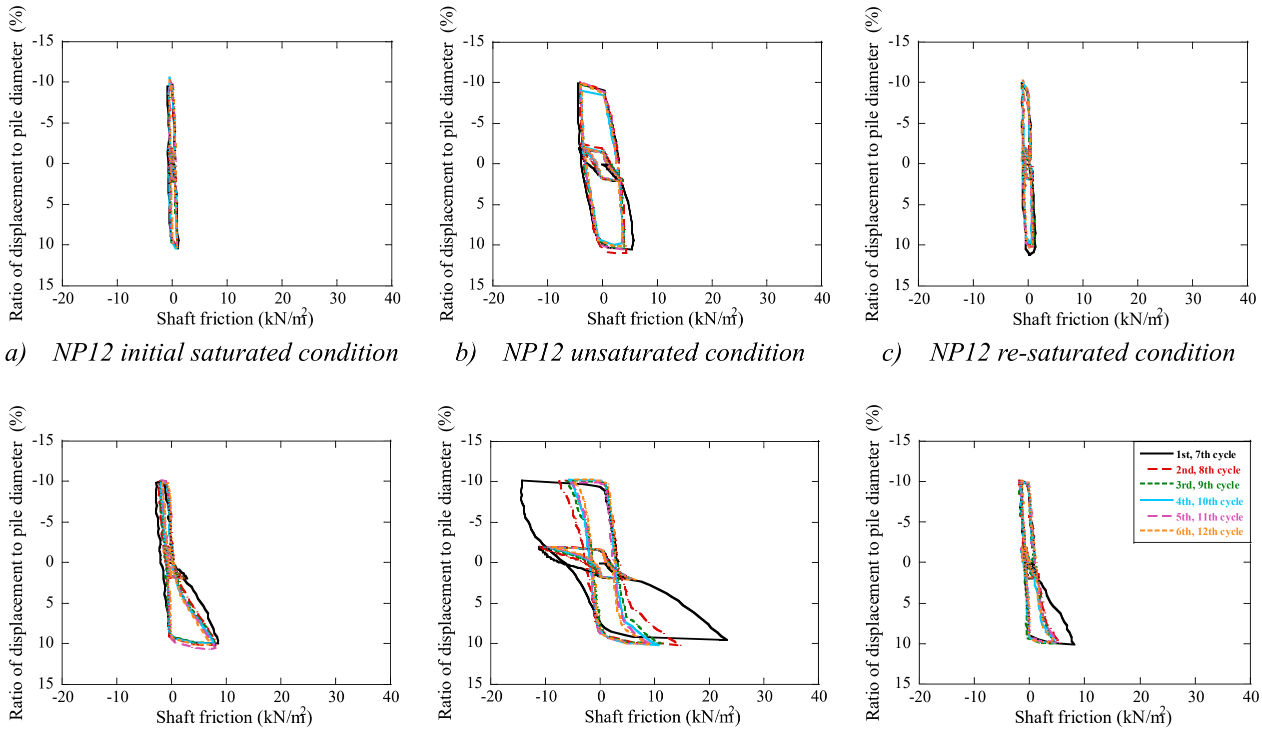

a) NP12 initial saturated condition *b) NP12 unsaturated condition* *c) NP12 re-saturated condition*

d) SP30 initial saturated condition *e) SP30 unsaturated condition* *f) SP30 re-saturated condition*

Figure 7. Shaft frictional resistance vs displacement ratio of NP12 and SP30 in saturated, unsaturated, and re-saturated sandy ground.

6c and 6f).

Figure 7 illustrates the relationship between shaft friction and displacement normalized by pile diameter. The spiral pile consistently exhibits significantly higher shaft friction than the normal pile, approximately three to four times greater in compression and two to three times greater in pull-out under both saturated and unsaturated conditions. This enhancement is attributed to the spiral configuration, which increases the contact area between the pile and surrounding soil (Wada et al., 2017, shah et al., 2024).

For the normal pile, shaft friction remains stable in saturated conditions, showing no notable degradation across loading cycles. In unsaturated conditions, it exhibits only slight degradation during the second loading sequence (Figure 7b). In contrast, the spiral pile shows more pronounced degradation, particularly under unsaturated conditions (Figure 7e). This reduction is attributed to the formation of a cyclic-loading-induced gap between the pile and soil. During cyclic loading, the spiral blades compact the surrounding sand, but suction holds the compacted sand in place, allowing relative slip along the pile surface and resulting in minimal shaft friction after several cycles.

Upon re-saturation, suction dissipates, allowing sand to flow and partially fill the gaps, which restores soil-pile contact and leads to partial recovery of shaft friction. However, as some sand also flows downward to fill the gap beneath the pile tip, lateral confinement around the shaft decreases. Consequently, the overall shaft friction after re-saturation remains lower than that in both the initial saturated and unsaturated states (Figures 7c and 7f).

4 CONCLUSIONS

Cyclic loading under unsaturated conditions induces a distinct degradation mechanism in both normal and spiral piles, characterized by the formation of a loading-induced gap at the pile-soil interface. This gap results from the asymmetric soil response during push-in and pull-out cycles, densification during compression followed by limited rebound during unloading. In unsaturated sand, matric suction prevents particle migration into this void, maintaining separation between the pile and soil and consequently reducing both tip resistance and shaft friction. Upon re-saturation, the dissipation of suction allows sand to flow into the gap, restoring continuous contact along the shaft and tip. The prior cyclic compaction also promotes localized densification, further enhancing interparticle interlocking. As a result, both pile types, particularly the spiral pile, exhibit partial to full recovery of capacity upon re-saturation, sometimes exceeding the initial saturated performance but remaining lower than that observed under unsaturated conditions.

These findings highlight that cyclic gap formation and suction-controlled recovery govern the mechanical behavior of piles in unsaturated sandy soils. In future work, it would be valuable to conduct a more detailed analysis incorporating specific suction and saturation values, perform DEM-based reproduction analyses, and develop parametric studies to integrate these mechanisms into practical design methods.

REFERENCES

Araki, K. (2013). Simplified foundation method subject to small-scale structure "PIN FOUNDATION METHOD." *The Japanese Geotechnical Society*, 61(8): 32-33 (in Japanese).

Bradshaw, A.S., Zuelke, R., Hildebrandt, L., Robertson, T. and Mandujano, R. (2018). Physical modelling of a helical pile installed in sand under constant crowd. *Proceedings of the 1st International Symposium on Screw Piles for Energy Applications (ISSPEA)*, pp. 109-115.

BSI (2015). BS 8004:2015 – Code of practice for foundations. London, UK: British Standards Institution.

Cerfontaine, B., Brown, M.J., Knappett, J.A., Davidson, C., Sharif, Y.U., Huisman, M., Ottolini, M. and Ball, J.D. (2023). Control of screw pile installation to optimise performance for offshore energy applications. *Géotechnique*, 73(3): 234-249. https://doi.org/10.1680/jgeot.21.00118

Cerfontaine, B., Knappett, J., Brown, M.J., Davidson, C. and Sharif, Y. (2020). Optimised design of screw anchors in tension in sand for renewable energy applications. *Ocean Engineering*, Vol. 217, 108010. https://doi.org/10.1016/j.oceaneng.2020.108010

Hirata, A., Kokaji, S. and Goto, T. (2005). Study on the estimation of the axial resistance of spiral bar based on interaction with ground. *Shigen-to-Sozai*, Vol. 121, pp. 370–377 (in Japanese).

Ho, H.M., Malik, A.A., Kuwano, J., Brasile, S., Tran, T.V. and Mazhar, M.A. (2022). Experimental and numerical study on pressure distribution under screw and straight pile in dense sand. *International Journal of Geomechanics*, 22(9): 1–13. https://doi.org/10.1061/(ASCE)GM.1943-5622.0002520

Lutenegger, A. J. (2016). Foundation Alternatives for Ground Mount Solar Panel Installations. Geotechnical and Structural Engineering Congress, pp. 1873-1885. https://doi.org/10.1061/9780784479742.160.

Nakagawa, S., Yamauchi, R., Isobe, K. and Tomisawa, K. (2018). Evaluation of bearing capacity of a small-diameter spiral pile subjected to combined load using model tests. *Proceedings of the 1st International Conference on Press-in Engineering*, Kochi, pp. 117–124. https://doi.org/10.50876/icpe.1.0_117.

Perko, H.A. (2009). *Helical piles: A practical guide to design and installation*. Hoboken, NJ, USA: John Wiley & Sons.

Sato, T., Harada, T., Iwasaki, N., Hayashi, S. and Ohtani, J. (2015). Effect of shaft rotation of spiral piles under its installation on vertical bearing capacity. *Japanese Geotechnical Journal*, 10(2): 253–265 (in Japanese).

Shah, F., Isobe, K., Eki, T. and Kawai, K. (2024). Evaluation of penetration resistance, vertical bearing capacity and pull-out resistance of small diameter spiral piles subjected to positive and negative alternating loads in unsaturated sandy ground. *Proceedings of the 3rd International Conference on Press-in Engineering (ICPE 2024)*, Singapore, pp. 72-80.

Sharif, Y.U., Brown, M.J., Cerfontaine, B., Davidson, C., Ciantia, M., Knappett, J., Brennan, A., Ball, J.D., Augarde, C., Coombs, W., Blake, A., Richards, D., White, D., Huisman, M. and Ottolini, M. (2021). Effects of screw pile installation on installation requirements and in-service performance using the discrete element method. *Canadian Geotechnical Journal*, 58(9): 1334–1350. https://doi.org/10.1139/cgj-2020-0241

Tamboura, H.H., Yamauchi, R. and Isobe, K. (2022). Bearing capacity evaluation of small-diameter spiral piles in soft ground subjected to combined loads. *Soils and Foundations*, 62(5): 101204. https://doi.org/10.1016/j.sandf.2022.101204

Ullah, S.N., Hu, Y. and O'Loughlin, C. (2019). A green foundation for offshore wind energy – helical piles. World Engineers Convention (WEC2019).

Wada, M., Tokimatsu, K., Maruyama, S. and Sawaishi, M. (2017). Effects of cyclic vertical loading on bearing and pullout capacities of piles with continuous helix wing. *Soils and Foundations*, 57(1): 141–153. https://doi.org/10.1016/j.sandf.2017.01.010.

Zhou, S., Zhou, M., Tian, Y. and Zhang, X. (2023). Effects of strain rate and strain softening on the installation of helical pile in soft clay. *Ocean Engineering*, Vol. 285, 115370. https://doi.org/10.1016/j.oceaneng.2023.115370